ՀՀ ԿՐԹՈՒԹՅԱՆ, ԳԻՏՈՒԹՅԱՆ, ՄՇԱԿՈՒՅԹԻ ԵՎ ՍՊՈՐՏԻ
ՆԱԽԱՐԱՐՈՒԹՅՈՒՆ
ԵՐԵՎԱՆԻ ՊԵՏԱԿԱՆ ՀԱՄԱԼՍԱՐԱՆ

ԱՍԱՏՐՅԱՆ ՀՐԱՉՅԱ ՀԱՅԿԻ

ՈՒԺԵՂ ՓՈԽԱԶԴԵՑՈՒԹՅՈՒՆՆԵՐԻ ՈՒՂՂՈՒՄՆԵՐԸ B-ՄԵԶՈՆԻ ԹՈՒՅԼ ՌԱԴԻԱՑԻՈՆ ՏՐՈՀՈՒՄՆԵՐԻ ՀԱՄԱՐ

Ա.04.02 - «Տեսական ֆիզիկա» մասնագիտությամբ
ֆիզիկամաթեմատիկական գիտությունների թեկնածուի
գիտական աստիճանի հայցման ատենախոսության

ՍԵՂՄԱԳԻՐ

ԵՐԵՎԱՆ - 2026

MINISTRY OF EDUCATION, SCIENCE, CULTURE AND SPORT OF THE
REPUBLIC OF ARMENIA
YEREVAN STATE UNIVERSITY

ASATRYAN HRACHYA

STRONG INTERACTION CORRECTIONS FOR WEAK RADIATIVE B-MESON DECAYS

Thesis for the degree of Candidate of physical and mathematical sciences
Speciality 01.04.02 - ”Theoretical Physics”

ABSTRACT

YEREVAN - 2026

Ատենախոսության թեման հաստատվել է Երևանի պետական համալսարանում

Գիտական ղեկավար՝	ֆիզ.-մաթ. գիտ. դոկտոր, պրոֆեսոր Ա.Ա. Սահարյան
Պաշտոնական ընդդիմախոսներ՝	ֆիզ.-մաթ. գիտ. դոկտոր Ռ.Հ. Պողոսյան ֆիզ.-մաթ. գիտ. դոկտոր, պրոֆեսոր Ս.Դ. Օդինցով
Առաջատար կազմակերպություն՝	ՀՀ ԳԱԱ Ֆիզիկայի Կիրառական Պրոբլեմների Ինստիտուտ

Ատենախոսության պաշտպանությունը կայանալու է 2026թ. մարտի 16-ին ժամը 14:30 Երևանի պետական համալսարանում գործող Ֆիզիկայի 049 Մասնագիտական խորհրդի նիստում:

Հասցե՝ 0025 Երևան, Ալեք Մանուկյան փ. 1, ԵՊՀ

Ատենախոսությանը կարելի է ծանոթանալ ԵՊՀ գրադարանում:

Սեղմագիրն առաքված է 2026թ. փետրվարի 12-ին:

Մասնագիտական խորհրդի գիտական քարտուղար՝  Դոցենտ Վ.Պ. Քալանթարյան

The thesis theme is approved at the Yerevan State University

Scientific supervisor:	Doctor of Phys. Math. Sciences Prof. A.A. Saharian
Official opponents:	Doctor of Phys. Math. Sciences R. H. Poghossian Doctor of Phys. Math. Sciences, Prof. S. D. Odintsov
Leading organization:	Institute of Applied Problems of Physics of NAS RA

The defense of the thesis will take place on March 16, 2026 at 14:30 in the session of the Specialized Council 049 Physics of the Yerevan State University.

Address: 1 Alex Manoogian Street, 0025 Yerevan, Armenia.

The thesis is available in the library of Yerevan State University.

The abstract is distributed on February 12, 2026.

Scientific secretary of the Specialized Council  Associate Professor V.P. Kalantaryan

GENERAL DESCRIPTION OF THE WORK

Relevance of topic. Rare flavor-changing neutral current (FCNC) decays of B mesons, such as the radiative transitions $B \to X_s\gamma$ and $B \to X_s\gamma\gamma$, play a central role in testing the Standard Model (SM) and probing potential new physics at scales far beyond the reach of current colliders. Since such processes are loop-surpressed in the Standard Model, they provide a sensitive probe of heavy virtual particles and higher-order quantum corrections. The inclusive decay rate of $B \to X_s\gamma$ is one of the most precisely measured observable quantities in flavor physics, with experimental uncertainties at only a few percent. To compare theoretical predictions with experimental averages, the next-to-next-to-leading order (NNLO) QCD corrections, which correspond to three-loop diagrams at order $\mathcal{O}(\alpha_s^2)$, must be calculated at a high precision.

While significant progress has been achieved over the past two decades [1, 2], a complete NNLO calculation at a physical charm mass has remained an open problem due to the enormous technical complexity of evaluating three-loop diagrams with two mass scales. The analytic and semi-analytic methods developed and applied in this work address this gap. The techniques used here (combining differential equation approaches, boundary condition evaluation through auxiliary mass flow, and matched asymptotic and Taylor expansions) provide a modern, numerically stable, and analytically transparent framework for the full computation of the $b \to s\gamma$ amplitude at $\mathcal{O}(\alpha_s^2)$. Accurate NNLO predictions for $B \to X_s\gamma$ are not only essential for precision tests of the Standard Model but also directly constrain a wide class of extensions, including supersymmetric models, two-Higgs-doublet models, and scenarios with vector-like quarks. Furthermore, the computational methods obtained in this work lay the foundation for future studies of related radiative decays such as $B \to X_s\gamma\gamma$, extending next-to-leading order (NLO) accuracy to multi-photon processes.

Among the important consequences of quantum field theory is the existence of nontrivial properties of the vacuum, defined as a state of quantum field with zero number of particles. An actively developing area is the investigation of the influence of external electromagnetic and gravitational fields on the properties of the vacuum. The interest is motivated by wide range of applications in condensed matter physics, micromechanical systems, gravitation, and cosmology. In several problems, the interaction of a field can be described by an effective model, in which boundary conditions are imposed on the field operator. The conditions modify the spectrum of zero-point fluctuations, resulting in changes to the expectation values of the physical observables. These types of effects have been investigated for various fields, boundary conditions, boundary and background geometries. Among the interesting points is the dependence of the physical observables on the mass of the field quanta. Motivated by applications in electromagnetism, the boundary-induced vacuum effects for vector fields have been studied mainly for the massless case. However, massive vector fields appear in a number of physical models. Of particular relevance are the gauge vector fields within the Standard Model. In electrodynamic systems, a photon can also acquire an effective mass, and the corresponding dynamics can be described in terms of a massive vector field model. These include electrodynamic models in media and theories with extra dimensions. The motivation to investigate quantum phenomena in the context of massive vector fields is also attributed to the potential non-zero mass of the photon.

The presented thesis pursues **two main goals**. In the **first part**, we perform a

complete evaluation of the radiative decay amplitude $b \to s\gamma$ at order $\mathcal{O}(\alpha_s^2)$ within the Standard Model for a physical value of the charm-quark mass, using modern analytic and semi-analytic techniques for the calculation of multi-loop Feynman diagrams. The ultimate aim of this part is to improve the NNLO precision for the inclusive decay rate $B \to X_s\gamma$, thus reducing the theoretical uncertainty to a level compatible with the expected increased experimental precision. In the **second part**, we investigate the properties of the vacuum state for a massive vector field in the geometry of two parallel plates on background of $(D+1)$-dimensional Minkowski spacetime. The two-point functions and the local characteristics of the vacuum state are studied for higher-dimensional generalizations of the perfect magnetic conductor (PMC) and perfect electric conductor (PEC) boundary conditions.

The following specific problems are considered:

- **Problem 1.** To develop and apply a systematic method for the calculation of three-loop diagrams contributing to $b \to s\gamma$ at $\mathcal{O}(\alpha_s^2)$.

- **Problem 2.** To implement the differential equation method for master integrals, including the derivation of boundary conditions using the auxiliary mass flow technique and their transport across the full physical range of $z = m_c^2/m_b^2$.

- **Problem 3.** To construct both asymptotic and Taylor expansions of the form factors in complementary kinematic regions and to establish a reliable "switched expansion" procedure ensuring numerical stability across the full physical range.

- **Problem 4.** To validate the obtained results through cross-comparison with independent computational frameworks and to prepare the groundwork for NLO calculations of related radiative decays such as $b \to s\gamma\gamma$.

- **Problem 5.** To investigate the properties of quantum vacuum for a massive vector fields in the presence of reflecting boundaries and to consider the zero-mass limit for comparison with the results in higher-dimensional generalization of Maxwell's electromagnetism.

Scientific novelty. The novelty of the present work lies in the first complete and fully systematic calculation of the three-loop ($\mathcal{O}(\alpha_s^2)$) contributions to the form factor decomposition of the $b \to s\gamma$ decay amplitude for diagrams involving the current-current operators O_1 and O_2, across the full range of the squared charm-to-bottom mass ratio $z = m_c^2/m_b^2$. The vacuum expectation values of physical observables characterizing the quantum vacuum for a massive vector field are investigated in the presence of reflecting boundaries with two types of conditions on parallel plates in background of $(D + 1)$-dimensional Minkowski spacetime.

The following aspects of the work constitute its main innovative contributions:

- For the first time, a complete set of three-loop diagrams containing at least one gluon attached to the b-quark line (the "b-leg diagrams'') and mixed topologies has been evaluated using the differential equation method combined with auxiliary mass flow techniques.

- The use of the `AMFlow` framework for determining boundary conditions of multi-scale master integrals at a specific kinematic point ($z = 1/100$), followed by numerical transport to the full physical range, provides a novel and highly precise computational strategy for heavy-flavor loop amplitudes.

- The construction of dual expansions: an asymptotic series around $z = 0$ and a Taylor expansion around $z = 1/10$, and their seamless matching through a "switched expansion" procedure is introduced as a robust approach to ensuring numerical stability across the physical domain $z \in [0.04, 0.16]$.

- The obtained results for the bare form factors B_{O_1} and B_{O_2} agree perfectly with recent independent findings, confirming both the reliability of the employed framework and its potential for generalization to higher-order or more complex decay processes.

- The developed methodology sets the foundation for future NNLO renormalization and phenomenological analysis of $B \to X_s\gamma$, as well as for next-to-leading order (NLO) studies of double-radiative decays such as $B \to X_s\gamma\gamma$.

- Complete set of mode functions for a massive vector field and the corresponding two-point functions are derived for PMC and PEC boundary conditions on parallel plates.

- Closed analytic expressions are provided for the local characteristics of the vacuum state and their asymptotic behavior is studied in limiting regions of the parameter values. The nature of the Casimir and Casimi-Polder forces is investigated.

Practical importance. The practical importance of the research lies in the development and validation of a computational framework capable of handling multi-scale, multi-loop amplitudes in heavy-flavor physics with high numerical precision. The obtained results for the $\mathcal{O}(\alpha_s^2)$ contributions to the $b \to s\gamma$ decay amplitude constitute a crucial part of the complete next-to-next-to-leading order (NNLO) theoretical prediction for the inclusive decay rate of $B \to X_s\gamma$. Such precision is essential for testing the Standard Model at the loop level and for constraining possible effects of physics beyond the Standard Model through flavor observables. Furthermore, the computational and methodological advances presented in the thesis, particularly the combined use of the differential equation and auxiliary mass flow methods, can be directly applied to a wide range of processes involving heavy quarks and electroweak loops, including $B \to X_s\gamma\gamma$ and related radiative decays. The established workflow allows for efficient and reproducible high-order perturbative calculations in quantum field theory, providing both practical and conceptual value to the broader field of precision flavor physics. The complete sets of modes for a massive vector field and the two-point functions can be used in investigations of various phenomena involving vector fields. The developed method for the separation of the boundary-induced contributions in the expectation values can also be used in problems with other boundary conditions.

The basic results to be defended are as follows:

1. The formulation of a complete and gauge-invariant decomposition of the $b \to s\gamma$ decay amplitude at order $\mathcal{O}(\alpha_s^2)$ in terms of the form factor B.

2. The full evaluation of all three-loop diagrams related to the current-current operators O_1 and O_2 (including b-leg, mixed, and bubble topologies) using differential equations and auxiliary mass flow techniques.

3. The construction of two complementary expansions of the amplitude: an asymptotic expansion around $z = 0$ and a Taylor expansion around $z = 1/10$, and their consistent matching across the physical domain through a switched expansion method.

4. The validation and cross-check of results with independent computational tools, establishing a numerically precise and stable framework for future NNLO analyses of $B \to X_s\gamma$ and related decays.

5. For a massive vector field in the geometry of two parallel plates the vacuum energy density is positive for PMC boundary conditions and becomes negative for PEC conditions.

6. The Casimir forces between two plates are attractive for both PMC and PEC boundary conditions. The Casimir-Polder forces, acting on a polarizable microparticle, are repulsive/attractive with respect to the nearest plate for PMC/PEC boundary conditions.

7. In the zero-mass limit the VEVs of the electric and magnetic field squares and the condensate reduce to the corresponding expressions for a massless vector field. The same holds for the VEV of the energy-momentum tensor in the problem with PEC conditions. For PMC conditions the zero-mass limit for the vacuum energy-momentum tensor differs from the corresponding VEV for a massless field.

Approbation of the work. The results of the thesis were reported at the conference "Annual Summary Conference - 2025" (Dilijan, 2025), and have been discussed at the seminars of the Chair of Theoretical Physics of Yerevan State University and of the University of Bern (Bern, Switzerland).

Publications. Five papers are published on the topic of the thesis.

Structure of the thesis. The thesis consists of an Introduction, three Chapters, a Conclusion, and the bibliography. It contains 139 pages, including 21 figures.

CONTENT OF THE THESIS

In the **Introduction**, a review of the scientific literature related to the subject of the thesis is presented. The relevance and motivation of the research are discussed, the aim and objectives of the work are formulated, and the scientific novelty and practical significance are outlined. The main results obtained in the thesis are also summarized.

In **Chapter 1**, the analytic approach to multi-loop Feynman diagram evaluation is described in detail. As an example, a representative pair of diagrams is selected from the radiative decay process $b \to s\gamma$, which is related to the O_2 and O_7 operators' interference. For this pair of diagrams, the amplitude is calculated entirely analytically.

The analytic calculation is based on the *method of differential equations*, which has become a cornerstone of modern multi-loop calculations in quantum field theory. The

method begins by expressing the amplitude corresponding to each diagram as a sum of scalar integrals using the program `Tracer`. This step systematically reduces the problem from one involving complex spinor algebra to one involving scalar Feynman integrals that depend only on the momenta and masses of the decay.

Once the scalar representation of the amplitude is obtained, the next step involves identifying relations among the large number of integrals generated. These relations are established through integration-by-parts (IBP) and Lorentz-invariance identities. The reduction of the complete set of scalar integrals to a smaller, linearly independent basis of so-called *master integrals* is carried out using Laporta's algorithm, as implemented in the publicly available package `Kira`, among others. This reduction is an essential step: while a typical three-loop diagram may contain hundreds or even thousands of scalar integrals, symmetry and IBP relations ensure that all of them can be expressed as linear combinations of a handful of master integrals.

Having identified the master integrals, the next step is to construct a system of first-order linear differential equations by differentiating each master integral with respect to the kinematic variables of the given problem. In the case of $b \to s\gamma$, this variable is the dimensionless ratio $z = m_c^2/m_b^2$, where m_b and m_c denote the bottom- and charm-quark masses, respectively. The derivatives of the master integrals with respect to z are themselves expressible as linear combinations of the same master integrals, with coefficients which are rational functions of z and the dimensional regularization parameter $\varepsilon = (4-d)/2$. This leads to a closed system of differential equations of the form

$$\frac{d}{dz}\vec{I}(z,\varepsilon) = A(z,\varepsilon)\,\vec{I}(z,\varepsilon),$$

where $\vec{I}$ is the vector of master integrals and $A(z,\varepsilon)$ is a rational matrix.

The feasibility of solving such systems crucially depends on the choice of basis for the master integrals. In general, the differential equation matrix $A(z,\varepsilon)$ has a complicated dependence on ε. However, it is often possible to find a new basis of integrals, known as a *canonical basis*, in which the system assumes the simplified "ε-form":

$$\frac{d}{dz}\,\vec{J}(z,\varepsilon) = \varepsilon\, A_c(z)\,\vec{J}(z,\varepsilon),$$

where $\vec{J}$ is the vector of master integrals in the canonical basis and $A_c(z)$ is independent of ε. In this form, the structure of the solution becomes transparent: the integrals can be expressed as iterated integrals, i.e. Generalized Polylogarithms (GPLs), whose arguments correspond to the singularities of $A_c(z)$. The algorithmic implementation of this transformation is performed using the package `CANONICA`.

Finding the canonical form has significant practical and conceptual advantages. Most importantly, it allows one to obtain analytic expressions valid to all orders in ε through purely algebraic integration of logarithmic forms. In the present work, the canonical transformation was successfully found for the selected two-loop topologies relevant to $b \to s\gamma$, leading to compact analytic expressions in terms of GPLs.

The power of these analytic frameworks was further demonstrated by their application to precision observables in neutral B-meson mixing. By retaining full charm-quark mass

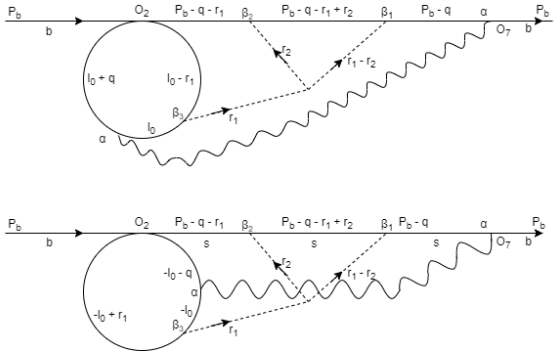

Figure 1: Representative diagrams from the decay $b \to s\gamma$ for which the analytic calculations were performed, illustrating the structure of the master integral reduction and the application of the differential equation method.

dependence, the analytic evaluation of penguin contributions at order $\mathcal{O}(\alpha_s^2 N_f)$ significantly reduced the theoretical uncertainty in the width difference and CP asymmetry. This confirms that for tractable topologies, analytic techniques remain the most robust tool for reducing theoretical errors. However, as is also discussed in the literature, such transformations are not always possible for more complex topologies. This practical limitation underlines one of the major challenges of purely analytic approaches.

Once the canonical system is obtained, the differential equations are integrated order-by-order in ε. The integration yields analytic expressions for each coefficient in the ε expansion, expressed as combinations of GPLs with arguments and weights determined by the structure of the matrix $A_c(z)$. The solutions are uniquely determined once appropriate boundary conditions are specified. These are typically fixed at kinematic points where the integrals simplify, such as $z \to \infty$.

In the second part of the chapter, the limitations of the fully analytic approach are discussed. As noted in [3], the complete set of three-loop Feynman diagrams contributing to the $b \to s\gamma$ amplitude from the current–current operators O_1 and O_2 at order α_s^2 was evaluated for the subset in which no gluon line is attached to the b-quark leg. In that work, the authors encountered topologies for which the transformation required to cast the differential equations into the canonical form could not be found. Consequently, these diagrams could not be solved analytically and had to be evaluated numerically using the sector decomposition method implemented in the program `FIESTA5`.

Given these challenges, and considering the rapid progress in recent years in numerical and semi-analytic techniques for the evaluation of multi-loop master integrals, a detailed comparative study was undertaken. The objective was to assess the performance, numerical precision, and practicality of modern methods against existing analytic benchmarks. To this end, a representative pair of diagrams, previously computed analytically in [3], was selected, and its master integrals were recalculated using several state-of-the-art tools: sector decomposition with `PySecDec`, auxiliary mass flow with

AMFlow, and differential equation solvers provided by both DiffExp and the DESolver module of AMFlow. The chapter also provides a brief discussion of two additional tools, FIESTA5 and SeaSyde, which were considered but ultimately excluded from the final comparison.

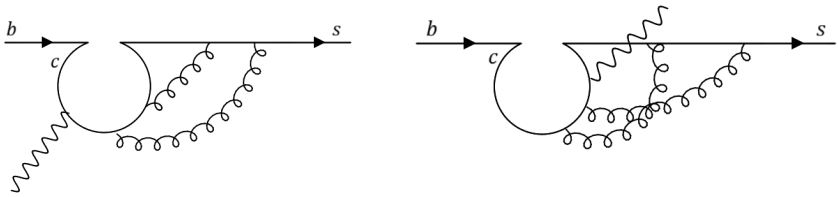

Figure 2: The two representative diagrams used for the comparative analysis of different computational approaches.

The quantitative comparison of methods is summarized in Table 1, while the corresponding graphical results are shown in Fig. 3. The table demonstrates that all differential-equation–based methods achieve excellent numerical precision, with AMFlow and DiffExp outperforming purely numerical approaches such as PySecDec. The graphical comparison further illustrates the convergence behavior of the various series expansions. Within their respective radii of convergence, all methods show near-perfect agreement with analytic results; however (as will be made apparent in the second chapter), no single expansion can simultaneously cover both the asymptotic region ($z \to 0$) and the physical region ($z \in [0.04; 0.16]$). Consequently, the combined use of two complementary expansions (typically an asymptotic expansion around $z = 0$ and a Taylor expansion around $z = 1/10$) is required to achieve full coverage of the physically relevant domain.

The study highlights the effectiveness of the modern semi-analytic approach, in which boundary conditions for the master integrals are computed via the auxiliary mass flow technique implemented in AMFlow, and the corresponding differential equations are solved using either DESolver or DiffExp. This hybrid framework offers both analytic control and high numerical precision, while maintaining computational efficiency even for complex topologies. The demonstrated reliability and robustness of this method underpin its application to the complete NNLO ($\mathcal{O}(\alpha_s^2)$) calculation of $b \to s\gamma$, presented in Chapter 2, and it is expected to play an equally important role in future studies, such as the evaluation of NLO ($\mathcal{O}(\alpha_s)$) corrections to the related process $b \to s\gamma\gamma$.

Chapter 2 is devoted to the complete calculation of the inclusive radiative decay $b \to s\gamma$ at order α_s^2. This process represents one of the most important flavor-changing neutral current (FCNC) transitions in the Standard Model, as it proceeds only through loop effects and therefore serves as a sensitive probe of virtual heavy-particle dynamics and possible new physics contributions. The achieved theoretical precision at this order is essential for matching the accuracy of present and forthcoming experimental results for the branching ratio $\mathcal{B}(B \to X_s\gamma)$.

Method	$z = 1/10$		$z = 1/100$	
	Rel. diff	Digits	Rel. diff	Digits
AMFlow exp. at $z = 1/10$	6.5×10^{-7}	6	1.0×10^{-5}	4
AMFlow asymptotic	6.5×10^{-7}	6	2.2×10^{-18}	17
Aux. mass flow AMFlow	6.5×10^{-7}	6	2.2×10^{-18}	17
Transport from $z = 1/100$	6.5×10^{-7}	6	2.2×10^{-18}	17
PySecDec	1.4×10^{-2}	2	7.5×10^{-3}	1
DiffExp exp. at $z = 1/10$	6.5×10^{-7}	6	6.8×10^{-5}	3

Table 1: Relative differences and digit-level agreement for various methods at $z = 1/10$ and $z = 1/100$.

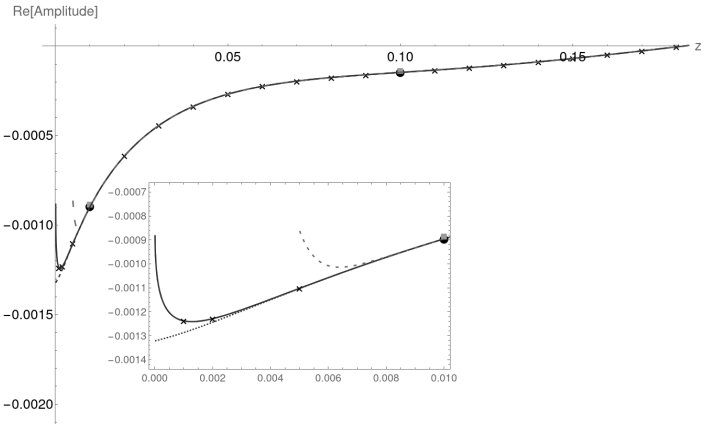

Figure 3: Real part of the coefficient of ε^0 for the O_1 contribution on the interval $z \in [0, 0.18]$. The main plot shows that over the entire physically important range $z \in [0.04; 0.16]$ the results of AMFlow (direct estimate •, transportation ×, Taylor expansion $\cdots$, asymptotic expansion $--$), DiffExp (---), and PySecDec (■) coincide with the analytical curve; the AMFlow asymptotic expansion completely overlaps the analytic curve (however, despite not being shown, it diverges as $z \to 0.2$), while both Taylor series diverge as $z \to 0$. The window shows the behavior in the region $z \leq 0.01$, where the divergence of the Taylor expansions and the stability of the asymptotic expansion coincidence are most clearly visible.

The calculation is carried out in the framework of the Weak Effective Theory (WET), where the heavy electroweak bosons and top quark are integrated out, and the short-distance physics is encoded in Wilson coefficients multiplying a basis of local operators. The dominant contributions at this order arise from the current–current operators O_1 and O_2, which mix into the electromagnetic dipole operator O_7 under renormalization. The corresponding matrix elements $\langle s\gamma|O_{1,2}|b\rangle$ contain the three-loop QCD corrections that form the focus of this chapter.

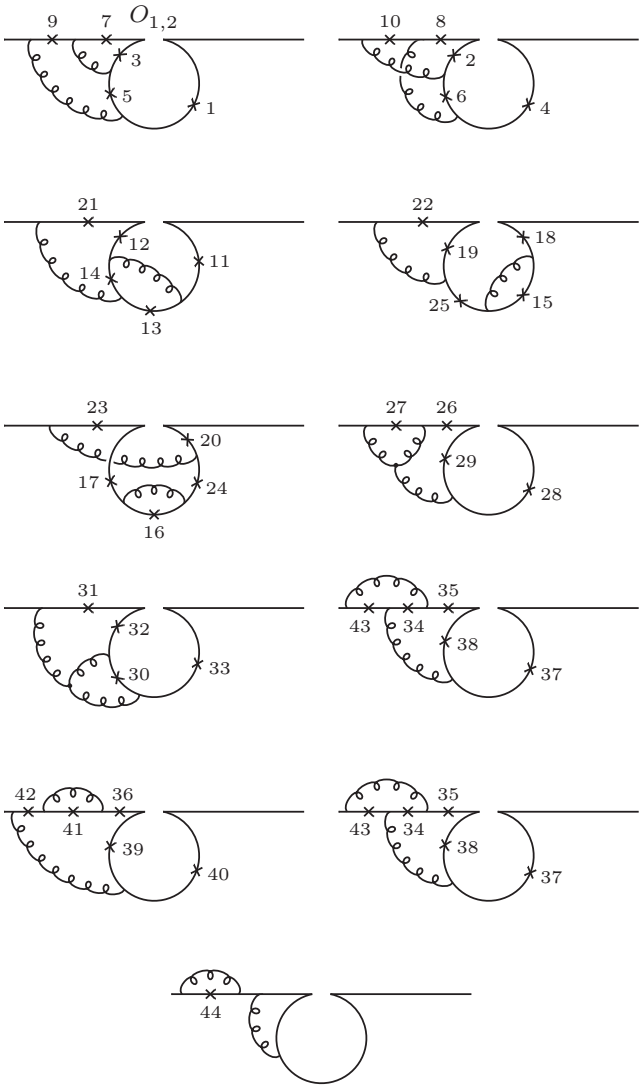

Figure 4: "b-leg diagrams": List of three-loop contributions to $b \to s\gamma$ associated with O_1 and O_2, where no gluon touches the s-leg. A cross on a quark line represents a possible place where the photon can be emitted. Only the diagrams which contribute to the form factor B are shown; they carry a diagram number next to the cross.

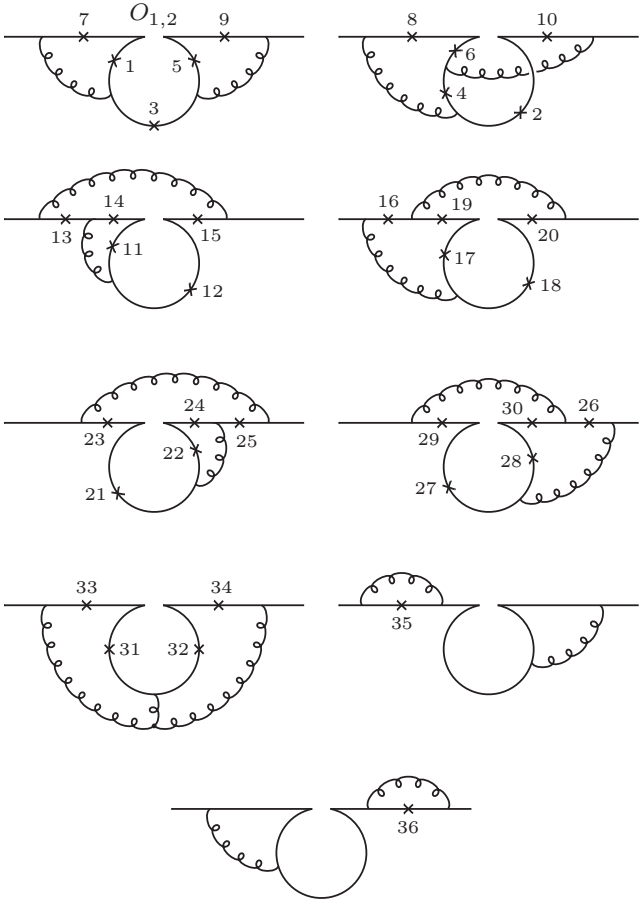

Figure 5: "Mixed diagrams": List of three-loop contributions to $b \to s\gamma$ associated with O_1 and O_2, where one gluon touches the b-leg and one touches the s-leg. A cross on a quark line represents a possible place where the photon can be emitted. Only the diagrams which contribute to the form factor B are shown.

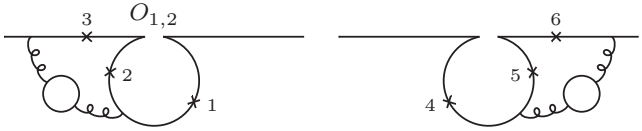

Figure 6: List of the "bubble diagrams" contributing to $b \to s\gamma$ associated with O_1 and O_2. A cross on a quark line represents a possible place where the photon can be emitted. Only the diagrams which contribute to the form factor B are shown.

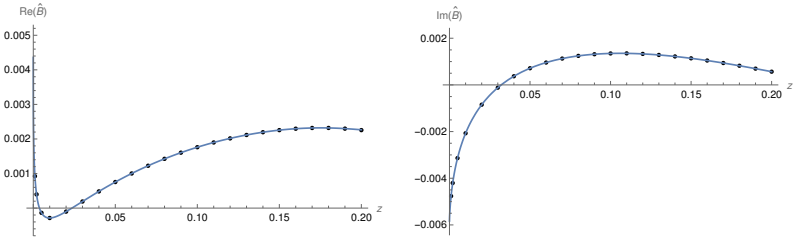

Figure 7: ϵ^0 coefficient of the O_2 contributions to the form factor B. The highlighted points are the 23 points mentioned in the text. The solid line is constructed by switching at $z = 0.04$ from the asymptotic expansion to the Taylor expansion.

The calculation follows a systematic form-factor decomposition of the decay amplitude, reducing it to a single physically relevant form factor B, as required by the QED Ward identity. All three-loop diagrams contributing to B are categorized into gauge-invariant subsets; namely, the "s-leg," (which have been calculated in [3]), "b-leg," "mixed," and "bubble" topologies, and each diagram is calculated using the methods outlined in Chapter 1.

Boundary conditions for all master integrals are computed with the auxiliary mass flow technique, implemented in the `AMFlow` package, at the reference point $z = 1/100$. The resulting high-precision boundary values are then numerically transported to 23 points covering the full kinematic range $z \in [10^{-3}, 0.2]$ using the `DESolver` module of `AMFlow`.

In addition to these numerical evaluations, analytic control is maintained through complementary expansions. Asymptotic expansions around $z = 0$ are constructed for all diagram classes using the boundary conditions at $z = 1/100$. However, the asymptotic expansions of certain "b-leg" topologies diverge near the physical region of z, and thus a Taylor expansion around $z = 1/10$ is also derived, using boundary conditions calculated by `AMFlow` at $z = 1/10$. The two expansions overlap smoothly at $z \approx 0.04$, providing a continuous and numerically stable description across the entire physically relevant range. Each expansion is carried out to order z^{20} or $(z - 1/10)^{20}$, with all logarithmic terms in the $z \to 0$ limit retained. This combined "switched expansion" technique ensures both precision and analytic transparency.

The final results for the dimensionless form factors B associated with the operators O_1 and O_2 are presented at the 23 reference points in z, together with the asymptotic values at $z \to 0$. The dependence on the dimensional regularization parameter ε is made explicit up to $\mathcal{O}(\varepsilon^0)$. The numerical stability of the results confirm the correctness and internal consistency of the full computation. The obtained results are in complete agreement with independent expansions published in [4].

In summary, this chapter presents the first complete and gauge-invariant evaluation of the $\mathcal{O}(\alpha_s^2)$ corrections to the matrix elements of O_1 and O_2 in the decay $b \to s\gamma$, including all topologies with gluon attachments to both quark legs and bubble insertions. The methodology combines analytic differential-equation techniques, auxiliary mass flow boundary conditions, and switched expansions in a unified framework. The resulting form factors constitute a critical component for the full NNLO prediction of $\mathcal{B}(B \to X_s\gamma)$, enabling precise tests of the Standard Model in the flavor sector.

The developed approach is fully generalizable and is expected to play a key role in forthcoming higher-order studies of related rare decays, such as $B \to X_s\gamma\gamma$, thereby extending the reach of precision flavor physics into the next generation of theoretical calculations.

Chapter 3 investigates vacuum polarization effects for the massive vector field A_μ in the presence of two parallel plates in $(D+1)$-dimensional Minkowski spacetime. This study generalizes the Casimir problem for vector fields beyond the massless (photon) case, providing a systematic analysis of how the finite mass and the number of spacetime dimensions affect the physical characteristics of the vacuum state. Such an analysis is of both conceptual and phenomenological interest: massive spin-1 fields naturally appear in various extensions of the Standard Model and in effective field-theoretical descriptions of condensed-matter systems and higher-dimensional models of gravity. The action for the field is given by

$$S = -\frac{1}{16\pi}\int d^{D+1}x\, \left[F_{\mu\nu}F^{\mu\nu} - 2m^2 A_\mu A^\mu\right], \tag{1}$$

where $F_{\mu\nu} = \partial_\mu A_\nu - \partial_\nu A_\mu$ is the field tensor. The mass term breaks the local gauge invariance of the theory. The corresponding field is known as the Proca vector field. In the Cartesian coordinates $x = (x^0, x^1, \ldots, x^{D-1}, x^D = z)$, the plates are located at $z = 0$ and $z = a$. Two types of boundary conditions are considered. The first condition corresponds to a higher dimensional generalization of PMC boundary conditions in Maxwell's electromagnetism and is expressed as $n^\nu F_{\mu\nu} = 0$ at $z = 0, a$, where n^ν is the normal to the plates. The second boundary condition is the analog of PEC condition and is formulated in terms of the dual tensor ${}^*F_{\mu_1\cdots\mu_{D-1}} = \varepsilon_{\mu\nu\mu_1\cdots\mu_{D-1}}F^{\mu\nu}/(D-1)!$ as $n^{\mu_1}\,{}^*F_{\mu_1\cdots\mu_{D-1}} = 0,\ z = 0, a$. The complete sets of the field modes are found for both types of boundary conditions. They describe states with $D-1$ transverse polarizations and a single state with longitudinal polarization. The PMC conditions act on all the polarizations, while the longitudinal polarization is not affected by the PEC conditions. As a consequence, the longitudinal polarization does not contribute to the boundary-induced VEVs of physical observables. By using the complete set of mode functions for the vector potential, the two-point functions $\langle 0|\, A_\mu(x)A_\nu(x')\,|0\rangle$ and $\langle 0|\, F_{\mu\nu}(x)F_{\rho\sigma}(x')\,|0\rangle$ are evaluated, with $|0\rangle$ being the vacuum state. These functions

describe the correlations of the vacuum fluctuations at different spacetime points. By using the Abel-Plana summation formula for the series over the component of the momentum normal to the plates, quantized by boundary conditions, the boundary-induced contributions in the two-point functions are explicitly separated. The divergences in the coincidence limit $x' \to x$ are contained in the boundary-free parts, and by their separation the renormalization of the VEVs of physical observables, quadratic in the field operator, is reduced to the one in the problem without boundaries.

As important physical characteristics of the vacuum state, the VEVs of the electric and magnetic fields squares, $\langle E^2 \rangle$ and $\langle B^2 \rangle$, the analog of the gluon condensate in QCD, $\langle F_{\mu\nu}F^{\mu\nu} \rangle$, and the VEV of the energy-momentum tensor, $\langle T_{\mu\nu} \rangle$, are evaluated by using the two-point functions. The vacuum energy-momentum tensor is diagonal and the vacuum energy density is equal to the stresses along the directions parallel to the plates. This property is a consequence of the invariance of the problem with respect to the Lorentz boosts along the directions parallel to the plates. The normal stress $\langle T_D^D \rangle$ does not depend on the z-coordinate and it vanishes in the geometry of a single plate. In the region between the plates, $0 < z < a$, and for the PMC conditions, the VEVs of the diagonal components of the energy-momentum tensor are given by (no summation over $l = 0, 1, \ldots, D-1$)

$$\begin{aligned}
\langle T_l^l \rangle &= \frac{m^{D+1}}{(2\pi)^{\frac{D+1}{2}}} \Bigg\{ -2D \sum_{n=1}^{\infty} f_{\frac{D+1}{2}}(2nma) \\
&\quad + (D-2) \sum_{n=-\infty}^{\infty} \Big[(D-1) f_{\frac{D+1}{2}}(2mz_n) + f_{\frac{D-1}{2}}(2mz_n) \Big] \Bigg\}, \\
\langle T_D^D \rangle &= \frac{2Dm^{D+1}}{(2\pi)^{\frac{D+1}{2}}} \sum_{n=1}^{\infty} \Big[D f_{\frac{D+1}{2}}(2nma) + f_{\frac{D-1}{2}}(2nma) \Big].
\end{aligned} \tag{2}$$

Here, $z_n = |z - na|$ and $f_\nu(x) = x^{-\nu} K_\nu(x)$, with $K_\nu(x)$ being the modified Bessel function of the second kind. For the PEC conditions the corresponding expressions read

$$\begin{aligned}
\langle T_l^l \rangle &= \frac{(1-D)\, m^{D+1}}{(2\pi)^{\frac{D+1}{2}}} \Bigg\{ 2 \sum_{n=1}^{\infty} f_{\frac{D+1}{2}}(2nma) \\
&\quad + \sum_{n=-\infty}^{\infty} \Big[(D-3) f_{\frac{D+1}{2}}(2mz_n) + \frac{D-2}{D} f_{\frac{D-1}{2}}(2mz_n) \Big] \Bigg\},
\end{aligned} \tag{3}$$

for $l = 0, 1, \ldots, D-1$, and for the normal stress one has $\langle T_D^D \rangle_{\rm PEC} = (D-1) \langle T_D^D \rangle_{\rm PMC} / D$. The ratio $(D-1)/D$ in this relation is the ratio of the number of polarization states influenced by the PEC and PMC boundary conditions. The $n = 0$ terms in the expressions for $\langle T_l^l \rangle$ correspond to the VEVs in the geometry with a single plate at $z = 0$. For $D \geq 3$, the vacuum energy density is found to be positive under PMC conditions and negative under PEC conditions, whereas for $D = 2$ the situation is reversed: the energy density is negative in the inter-plate region for PMC boundaries and vanishes elsewhere, while for PEC conditions it becomes positive. In one spatial dimension, the

energy density is negative everywhere for PMC conditions and vanishes for PEC conditions, demonstrating a highly nontrivial dimensional dependence of the vacuum structure. These results provide a unified description of how dimensionality and boundary constraints jointly determine the sign and distribution of vacuum energy. The Casimir force per unit surface of the plates (the Casimir pressure) is determined by the normal stress as $p_{\mathrm{C}} = -\langle T_D^D \rangle$. It is zero in the regions $z < 0$ and $z > a$ and is negative for the region between the plates. This corresponds to the attractive Casimir force. Hence, similar to the standard electromagnetic Casimir effect for parallel conducting plates, the attractive Casimir force is a consequence of a negative vacuum pressure in the region $0 < z < a$. In addition to the Casimir forces, the Casimir-Polder (CP) forces acting on a polarizable test particle placed near the plates are studied. For PMC boundary conditions, these forces are repulsive relative to the nearest plate, whereas for PEC boundary conditions they are attractive for $D \geq 2$ and vanish in one spatial dimension ($D = 1$). The qualitative difference in CP interaction behavior traces back to the distinct treatment of the longitudinal mode by the two types of boundaries.

The zero-mass limit of the obtained results is studied. For the PEC conditions, the VEVs of the electric and magnetic field squares, the field condensate, and the energy-momentum tensor all smoothly reduce to the results in quantum electrodynamics with zero-mass photon. For PMC boundary conditions, however, a qualitative difference emerges: while the VEVs of field squares and condensate approach their massless limits, the energy-momentum tensor does not. This discrepancy originates from the different role played by the longitudinal polarization mode of the massive vector field. Under PMC conditions, all polarization modes - including the longitudinal one - are subject to boundary constraints, whereas under PEC conditions the longitudinal mode remains unaffected by the plates. As a result, the PMC and PEC systems possess distinct vacuum structures in the zero-mass limit.

CONCLUSIONS

1. A comprehensive framework for the analytic and semi-analytic evaluation of multi-loop Feynman diagrams was developed and tested on representative topologies relevant to the radiative decay process $b \to s\gamma$. The method, based on the differential equation approach and the transformation of master integrals into a canonical basis, allows the derivation of fully analytic expressions in terms of Generalized Polylogarithms (GPLs) wherever such a transformation is attainable. For cases where analytic canonicalization was not feasible, modern semi-analytic and numerical methods were systematically compared, including `AMFlow`, `DiffExp`, and `PySecDec`. The comparative study demonstrated that `AMFlow` and `DiffExp` achieve precision comparable to analytic solutions, while fully numerical methods such as `PySecDec` show reduced accuracy for higher-loop integrals. This benchmarking provided a clear understanding of the reliability and practical limitations of each computational approach.

2. The results of this methodological investigation were then applied to the calculation of the three-loop ($\mathcal{O}(\alpha_s^2)$) contributions to the decay amplitude for $b \to s\gamma$ associated with the current–current operators O_1 and O_2 for arbitrary values of

the charm-quark mass m_c. Using `AMFlow`, all diagrams with at least one gluon attached to the b-quark leg, as well as those containing gluon self-energy insertions, were computed with high numerical precision across a wide range of $z = m_c^2/m_b^2$. For all integrals, boundary conditions were established via the auxiliary mass flow technique at $z = 1/100$ and $z = 1/10$, enabling stable numerical solutions of the corresponding differential equations between $z = 1/1000$ and $z = 1/5$. The program `DiffExp` and `AMFlow`'s `DESolver` package were used to construct an asymptotic expansion using the boundary conditions at $z = 1/100$, as well as a Taylor expansion around $z = 1/10$ using boundary conditions at $z = 1/10$.

3. A combined "switched expansion" was constructed by switching from the asymptotic expansion to the Taylor expansion around $z = 0.04$ to ensure convergence in the entire physical region of z. These results extend previous NNLO computations by completing the remaining topologies required for a full $\mathcal{O}(\alpha_s^2)$ prediction of the inclusive $B \to X_s\gamma$ branching ratio at physical charm mass. The methods developed here open the way to refine the precisions of other rare decays, notably $B \to X_s\gamma\gamma$, where it is expected to help calculate NLO ($\mathcal{O}(\alpha_s)$) results.

4. Vacuum polarization effects for a massive vector (Proca) field in the presence of parallel plates were investigated in $(D + 1)$-dimensional Minkowski spacetime. Exact expressions were derived for the two-point functions, vacuum expectation values of the field squares, and the energy-momentum tensor under both perfect electric conductor (PEC) and perfect magnetic conductor (PMC) boundary conditions. The analysis revealed nontrivial dependence of the vacuum structure on field mass, spacetime dimension, and boundary type, generalizing the Casimir effect to massive spin-1 fields in arbitrary dimensions.

5. For PMC boundaries, the longitudinal polarization mode was shown to play a decisive role, leading to qualitative differences in the zero-mass limit compared to the massless case and to PEC boundaries. The corresponding Casimir forces were found to be attractive for both boundary conditions, while the Casimir-Polder forces acting on a polarizable particle were repulsive for PMC and attractive for PEC conditions. The sign and spatial distribution of the vacuum energy density were found to depend sensitively on the number of spatial dimensions, revealing new insights into the interplay between geometry, mass, and dimensionality in vacuum field theory.

REFERENCES

1. M. Misiak, H. M. Asatrian, K. Bieri, M. Czakon, A. Czarnecki, T. Ewerth, A. Ferroglia, P. Gambino, M. Gorbahn, C. Greub, U. Haisch, A. Hovhannisyan, T. Hurth, A. Mitov, V. Poghosyan, M. Ślusarczyk, and M. Steinhauser, *Estimate of $\mathcal{B}(\bar{B} \to X_s\gamma)$ at $O(\alpha_s^2)$*, Phys. Rev. Lett. **98**, 022002 (2007).

2. M. Misiak, H. M. Asatrian, R. Boughezal, M. Czakon, T. Ewerth, A. Ferroglia, P. Fiedler, P. Gambino, C. Greub, U. Haisch, T. Huber, M. Kamiński, G. Ossola, M. Poradziński, A. Rehman, T. Schutzmeier, M. Steinhauser, and J. Virto, *Updated NNLO QCD predictions for the weak radiative B-meson decays*, Phys. Rev. Lett. **114**, no.22, 221801 (2015).

3. C. Greub, H.M. Asatrian, F. Saturnino, C. Wiegand, *Specific three-loop contributions to $b \to s\gamma$ associated with the current-current operators*, JHEP **05** (2023), 201.

4. M. Fael, F. Lange, K. Schönwald and M. Steinhauser, *Three-loop $b \to s\gamma$ vertex with current-current operators*, JHEP **11** (2023), 166.

PUBLICATIONS ON THE TOPIC OF THE THESIS

1. H. M. Asatrian, H. H. Asatryan, A. Hovhannisyan, U. Nierste, S. Tumasyan and A. Yeghiazaryan, *Penguin contribution to the width difference and CP asymmetry in B_q-$\bar{B}_q$ mixing at order $\alpha_s^2 N_f$*, Phys. Rev. D **102** (2020), 033007.

2. H. H. Asatryan and H. M. Asatrian, *Calculations of Higher Order Quantum Chromodynamics Corrections*, J. Contemp. Phys. **56** (2021) no.3, 177–183.

3. C. Greub, H. M. Asatrian, H. H. Asatryan, L. Born, and J. Eicher, *Three-loop contributions to $b \to s\gamma$ associated with the current-current operators*, JHEP **11** (2024), 058.

4. H. H. Asatryan, *Comparison of Various Feynman Diagram Calculation Methods for the Decay $b \to s\gamma$*, J. Contemp. Phys. **60** (2025) no.2, 131–136.

5. A. A. Saharian and H. H. Asatryan, *Two-point functions and the vacuum densities in the Casimir effect for the Proca field*, Eur. Phys. J. Plus **141** (2026), 106

ԱՄՓՈՓԱԳԻՐ

Ատենախոսությունում հետազոտված է $b \to s\gamma$ հազվագյուտ տրոհումը: Ուսումնասիրվել են Ֆեյնմանի դիագրամների հաշվարկի տարբեր մեթոդներ և կատարվել է թվային կամ կիսաթվային մեթոդների համեմատություն անալիտիկ արդյունքների հետ: Օգտագործելով նորագույն `AMFlow` և `DiffExp` ծրագրերը՝ հաշվարկվել է $b \to s\gamma$ տրոհման՝ O_1 և O_2 օպերատորների α_s^2 կարգի ներդրումները c-քվարկի զանգվածի ֆիզիկական արժեքների համար՝ ներկայացնելով արդյունքները որպես $z = m_c^2/m_b^2$ փոփոխականից շարքեր՝ $z = 0$ և $z = 1/10$ կետերի շուրջ: Ատենախոսությունում նաև հետազոտվել է զանգվածեղ Պրոկայի դաշտի վակուումային բևեռացման էֆեկտները զուգահեռ թիթեղների $(D+1)$-չափանի Մինկովսկու տարածաժամանակում:

1. Մշակվել և փորձարկվել է բարձր օղականի Ֆեյնմանի դիագրամների անալիտիկ և կիսաանալիտիկ հաշվարկի համապարփակ մեթոդաբանություն, որը կիրառվել է $b \to s\gamma$ ռադիացիոն տրոհման ներկայացուցչական դիագրամների վրա: Մեթոդը հիմնված է դիֆերենցիալ հավասարումների մեթոդի և վարպետ ինտեգրալների՝ կանոնիկ բազիսի տեղափոխման վրա, ինչը թույլ է տալիս ստանալ անալիտիկ արտահայտություններ՝ ընդհանրացված պոլիլոգարիթմների (GPL) տեսքով՝ այն դեպքերում, երբ նման կանոնականացում հնարավոր է:

2. Այն դեպքերի համար, երբ կանոնիկ բազիսի բերումը տեխնիկապես հնարավոր չէր, համակարգված կերպով համեմատվել են ժամանակակից կիսաանալիտիկ և թվային մեթոդները՝ `AMFlow`, `DiffExp` և `PySecDec` փաթեթները: Համեմատական ուսումնասիրությունը ցույց է տվել, որ `AMFlow`-ն ու `DiffExp`-ը թույլ են տալիս ստանալ անալիտիկ լուծումներին համարժեք ճշտություն, մինչդեռ թվային մեթոդները, ինչպիսին է օրինակ `PySecDec`-ը, ունեն ցածր ճշտություն բարձր օղականի ինտեգրալների համար: Այս համեմատությունը հնարավորություն է տվել գնահատելու յուրաքանչյուր մեթոդի հուսալիությունն ու կիրառելիության սահմանները:

3. Ուսումնասիրության արդյունքները կիրառվել են $b \to s\gamma$ տրոհման ամպլիտուդայի երեք-օղականի ($\mathcal{O}(\alpha_s^2)$) ներդրումների հաշվարկի մեջ՝ կապված O_1 և O_2 հոսանք–հոսանք օպերատորների հետ՝ c-քվարկի m_c զանգվածի կամայական ֆիզիկական արժեքի դեպքում: `AMFlow`-ի միջոցով բարձր ճշտությամբ հաշվարկվել են բոլոր այն դիագրամները, որոնք պարունակում են գոնե մեկ գլյուոնային գագաթ b-քվարկի գծի վրա, ինչպես նաև գլյուոնի սեփական էներգիայի հետ կապված դիագրամները՝ $z = m_c^2/m_b^2$ փոփոխականի լայն տիրույթում:

4. Բոլոր ինտեգրալների համար օժանդակ զանգվածի հոսքի մեթոդով որոշվել են եզրային պայմաններ $z = 1/100$ և $z = 1/10$ կետերում, ինչը հնարավորություն է տվել ստանալ կայուն թվային լուծումներ դիֆերենցիալ հավասարումների համար $z = 1/1000$–ից մինչև $z = 1/5$ միջակայքում: `DiffExp` ծրագիրը և `AMFlow`-ի `DESolver` փաթեթը կիրառվել ստանալու ասիմպտոտիկ վերլուծություն՝ օգտագործելով $z = 1/100$ կետում եզրային պայմանները, ինչպես նաև $z = 1/10$ կետի շուրջ Թեյլորի վերլուծություն՝ օգտագործելով $z = 1/10$ կետում եզրային պայմանները:

5. Կառուցվել է «փոխարկված» շարք (switched expansion), որը ստացվել է $z \approx 0.04$ կետում անցում կատարվելով ասիմպտոտիկ շարքից Թեյլորի շարքի: Այս

շարքի կառուցումը ապահովում է z փոփոխականի ֆիզիկական ռեջ տիրույթում արդյունքների բարձր ճշտություն: Այս արդյունքները շարունակում են անցյալում կատարված ԱԼՀՀ հաշվարկները՝ հաշվելով այն մնացած տոպոլոգիաները, որոնք անհրաժեշտ են $B \to X_s\gamma$ ինքլյուզիվ տրոհման $\mathcal{O}(\alpha_s^2)$ կարգի ամբողջական հաշվարկի համար՝ c-քվարկի ֆիզիկական զանգվածի համար:

6. Մշակված մեթոդները հնարավորություն են տալիս այլ հազվագյուտ տրոհումների բարձր ճշտությամբ հաշվարկների, մասնավորապես $B \to X_s\gamma\gamma$ տրոհման, որտեղ մշակված մեթոդի կիրառմամբ ակնկալվում է հաշվարկել NLO ($\mathcal{O}(\alpha_s)$) կարգի ուղղումներ:

7. Հետազոտվել է վակուումի բևեռացման երևույթը զանգվածեղ վեկտորական (Պրոկայի) դաշտի համար հարթ զուգահեռ թիթեղների առկայությամբ: Տարածական չափողականության ընդհանուր դեպքում ստացվել են ճշգրիտ արտահայտություններ դաշտի Երկկետային ֆունկցիաների, էլեկտրական ու մագնիսական դաշտերի քառակուսիների և էներգիա-իմպուլսի թենզորի վակուումային միջինների համար՝ թիթեղների վրա իդեալական մագնիսական հաղորդչի (PMC) և իդեալական էլեկտրական հաղորդչի (PEC) եզրային պայմանների դեպքերում: Վերլուծությունը բացահայտել է վակուումի հատկությունների ոչ տրիվիալ կախվածությունը դաշտի զանգվածից, տարածության չափողականությունից և եզրային պայմանից՝ ընդհանրացնելով Կազիմիրի էֆեկտի համար արդյունքները կամայական չափողականությունում զանգվածեղ սպին-1 դաշտերի համար:

8. PMC եզրային պայմանի ազդեցությունը երկայնական բևեռացմամբ վակուումային ֆլուկտուացիաների վրա վճռորոշ դեր է խաղում, զրոյական զանգվածի սահմանում հանգեցնելով որակական տարբերությունների՝ համեմատած Մաքսվելյան վեկտորական դաշտի և PEC պայմանով զանգվածեղ վեկտորական դաշտի հետ: Թիթեղների վրա ազդող Կազիմիրի ուժերը ձգողական են երկու տիպի սահմանային պայմանների համար, մինչդեռ բևեռացվող մասնիկի վրա ազդող Կազիմիր-Պոլդերի ուժերը վանողական են մոտակա թիթեղի նկատմամբ PMC համար և ձգողական՝ PEC պայմանի դեպքում: Վակուումային էներգիայի խտության նշանը և տարածական բաշխումը զգայունորեն կախված են տարածական չափողականությունից: Երեք և ավելի տարածական չափողականություններում վակուումի էներգիայի խտությունը դրական/բացասական է PMC/PEC պայմաններով թիթեղների համար:

АСАТРЯН ГРАЧЬЯ

ПОПРАВКИ СИЛЬНЫХ ВЗАИМОДЕЙСТВИЙ ДЛЯ СЛАБЫХ РАДИАЦИОННЫХ РАСПАДОВ B-МЕЗОНОВ

В диссертации исследован редкий распад $b \to s\gamma$. Изучены различные методы вычисления диаграмм Фейнмана (в частности, аналитический метод), а также выполнено сравнение других численных и полуаналитических методов с аналитическими результатами. С использованием современных пакетов `AMFlow` и `DiffExp` были вычислены вклады операторов O_1 и O_2 порядка α_s^2 в распад $b \to s\gamma$ для физических значений массы с-кварка, представленные в виде разложений по переменной $z = m_c^2/m_b^2$ в окрестностях точек $z = 0$ и $z = 1/10$. Кроме того, в диссертации исследованы эффекты вакуумной поляризации массивного векторного поля Проки в присутствии параллельных пластин в $(D + 1)$-мерном пространстве-времени Минковского. Получены точные выражения для двухточечных функций, вакуумных средних квадратов полей и тензора энергии–импульса.

1. Была разработана и протестирована всесторонняя методология аналитического и полуаналитического вычисления многопетлевых диаграмм Фейнмана на представительных топологиях, связанных с радиационным распадом $b \to s\gamma$. Подход основан на методе дифференциальных уравнений и преобразовании мастер интегралов в канонический базис, что позволяет получать полностью аналитические выражения в терминах обобщённых полилогарифмов (GPLs), когда такое преобразование возможно.

2. Для случаев, когда аналитическая канонизация недостижима, были систематически сравнены современные полуаналитические и численные методы, включая пакеты `AMFlow`, `DiffExp` и `PySecDec`. Сравнительное исследование показало, что `AMFlow` и `DiffExp` достигают точности, сопоставимой с аналитическими решениями, тогда как полностью численные методы, такие как `PySecDec`, демонстрируют более низкую точность для интегралов более высоких порядков. Это сравнение позволило чётко оценить надёжность и практические ограничения каждого вычислительного подхода.

3. Результаты этой методологической части работы были затем применены к вычислению вкладов трёхпетлевых ($\mathcal{O}(\alpha_s^2)$) диаграмм в амплитуду распада $b \to s\gamma$, связанных с ток–ток операторами O_1 и O_2, для произвольных значений массы с-кварка m_c. Используя `AMFlow`, с высокой численной точностью были вычислены все диаграммы, содержащие хотя бы один глюон, присоединённый к b-кварковой линии, а также диаграммы с глюонными вставками собственной энергии, во всём диапазоне $z = m_c^2/m_b^2$.

4. Для всех интегралов граничные условия были установлены с помощью техники вспомогательного массового расхода в точках $z = 1/100$ и $z = 1/10$, что обеспечило устойчивые численные решения соответствующих дифференциальных уравнений в интервале $z = 1/1000$ до $z = 1/5$. Пакеты `DiffExp` и `DESolver` из `AMFlow` были использованы для построения асимптотического разложения с граничными условиями при $z = 1/100$, а также ряда Тейлора вокруг $z = 1/10$ с граничными условиями при $z = 1/10$.

5. Было построено комбинированное «переключаемое разложение», заключающееся в переходе от асимптотического разложения к разложению Тейлора в области $z \approx 0.04$, что обеспечивает сходимость для всей физической области z. Полученные результаты

расширяют предыдущие NNLO-вычисления, завершая оставшиеся топологии, необходимые для полного предсказания порядка $\mathcal{O}(\alpha_s^2)$ для ширины распада $B \to X_s\gamma$ при физической массе с-кварка.

6. Разработанные методы открывают путь к повышению точности расчётов и для других редких распадов, в частности $B \to X_s\gamma\gamma$, где ожидается достижение точности на уровне NLO ($\mathcal{O}(\alpha_s)$).

7. Исследовано явление вакуумной поляризации для массивного векторного поля (поле Прока) в присутствии плоских параллельных пластин. В общем случае пространственной размерности получены точные выражения для двухточечных функций поля, вакуумных средних квадратов электрического и магнитного полей, а также вакуумного среднего тензора энергии-импульса в случаях граничных условий идеального магнитного проводника (PMC) и идеального электрического проводника (PEC) на пластинах. Анализ выявил нетривиальную зависимость свойств вакуума от массы поля, размерности пространства и граничного условия, обобщая результаты для эффекта Казимира для массивных полей со спином 1 в произвольной размерности пространства.

8. Влияние граничного условия PMC на вакуумные флуктуации с продольной поляризацией играет решающую роль, приводя к качественным различиям в пределе нулевой массы по сравнению с максвелловским векторным полем и массивным векторным полем с граничным условием PEC. Силы Казимира, действующие на пластины, являются притягивающими для обоих типов граничных условий, в то время как силы Казимира-Польдера, действующие на поляризуемую частицу, являются отталкивающими по отношению к ближайшей пластине для условия PMC и притягивающими для условия PEC. Знак и пространственное распределение плотности энергии вакуума сильно зависят от пространственного измерения. В трех или более пространственных измерениях плотность энергии вакуума положительна/отрицательна для пластин с граничными условиями PMC/PEC.